buildings

Article

Improving the Indoor Environment through an Indoor Green Curtain System

Ghulam Qadir [1,*], Niranjika Wijesooriya [2], Arianna Brambilla [2] and Fernando Alonso-Marroquin [1]

[1] School of Civil Engineering, The University of Sydney, Sydney, NSW 2006, Australia; fernando.alonso@sydney.edu.au
[2] School of Architecture, Design and Planning, The University of Sydney, Sydney, NSW 2006, Australia; arianna.brambilla@sydney.edu.au (A.B.)
* Correspondence: ghulam.qadir@sydney.edu.au

Abstract: People are spending more and more of their lives indoors, making thermal comfort and air quality essential factors for their health and well-being. The use of natural elements within indoor spaces can improve the indoor environment and air quality, but can also bring multiple health and well-being, psychological, cognitive, and behavioral benefits due to its biophilic effect. Indoor vertical greenery strategy in buildings can give these benefits to the building occupants. In this study, a prototype of a living green curtain is assessed to evaluate the benefits that may derive when used as a shading device. The analysis evaluated the performance of the green curtain prototype compared to the other two scenarios, no curtains (control module) and external blind. Temperature, relative humidity, air quality, and solar radiation were measured in the indoor environment. Results indicate that the green curtain module was cooler by 0–4 °C than the control module during the peak solar radiation hours, and the difference even reached up to 8 °C on hotter days. Due to the evapotranspiration effect, the green curtain recorded the highest daily average relative humidity of 67%. This study demonstrates the potential ability of a green curtain to improve air quality and thermal comfort.

Keywords: greening system; air quality; thermal comfort; green buildings; indoor environmental quality; prototype; biophilic design; biophilia

Citation: Qadir, G.; Wijesooriya, N.; Brambilla, A.; Alonso-Marroquin, F. Improving the Indoor Environment through an Indoor Green Curtain System. *Buildings* **2023**, *13*, 1307. https://doi.org/10.3390/buildings13051307

Academic Editors: Guangyu Wang, Jiang Liu, Xin-Chen Hong, Jinda Qi, Bao-Jie He and Shi Cheng

Received: 9 April 2023
Revised: 10 May 2023
Accepted: 15 May 2023
Published: 17 May 2023

1. Introduction

The rapid increase in urbanization has created several environmental issues, including the urban heat island effect [1], increased air pollution [2], increased temperature [3], and depletion of resources [4,5]. These negative effects add to climate change. In the urban environment, the high building density consumes more resources as the building sector accounts for 40% of the world's energy usage [6], mainly due to the high conditioning energy loads. Heating, ventilating, and air conditioning (HVAC) systems consume approximately 50–70% of the building energy, primarily because of inefficient building service systems and poorly insulated external walls [7]. The other reason for this high consumption lies in the control strategy, which was identified as a parameter that has a high potential to affect energy efficiency [8]. Therefore, reducing energy demand for heating and cooling is essential for improving the energy efficiency of a building, but modern technology re-circulates the air instead of refreshing it, which leads to reduced air quality [9]. Inadequate ventilation results in poor indoor air quality (IAQ) [10]. IAQ represents attributes of the respirable air inside a building (indoor climate), including gaseous composition, humidity, temperature, and contaminants [11]. With people spending 90% of their time inside buildings [12], IAQ is an essential factor contributing to people's health, comfort, and well-being. Indeed, poor IAQ can result in lower productivity and dissatisfaction in the workplace [13]. On the contrary, better IAQ can enhance the lives of building occupants, increase the resale value of the building, and reduce liability for building owners [14].

Recently, extreme events (e.g., bushfires and the COVID-19 pandemic) are forcing people to spend even more time indoors and persuading the building operation strategies to isolate the indoor environment. In addition, to keep the indoor environment healthy, the implementation of biophilic design strategies is important [15], because, during the building life cycle, the emissions of carbon dioxide is more than in the construction phase [16] and a biophilic design can minimize these emissions. The biophilic design uses natural elements on the premise to enhance human–nature connectedness which could immensely contribute towards health and well-being. The use of natural elements providing biophilic visual connections inside the building can improve IAQ as a factor of indoor environmental quality (IEQ) [17], as IEQ is defined by the American Society of Heating, Refrigerating and Air-conditioning Engineers (ASHRAE) [18] as "a perceived indoor experience of the building's indoor environment that includes aspects of design, analysis, and operation of energy-efficient, healthy and comfortable buildings". Consistently occupying spaces with natural elements can have positive effects on mood and cognitive performance [19], low pulse rates [20], and psychological nervousness (mental stress) [21], and it can also slow down blood flow, which minimizes the burden on the heart and, potentially preventing cardiovascular and cerebrovascular diseases [21]. Green plants also have a soothing effect on the human mind causing relaxation of the nervous system, reduction of mental stress, and fatigue prevention [22].

In recent decades, different internal and external vertical greening systems have spread worldwide. There are several terms used to define and describe vegetated vertical surfaces or green surfaces in buildings. Wall vegetation primarily refers to free-standing walls, and dividing properties [23]. Green or greened facades commonly feature woody or herbaceous climbers either planted into the ground or in planter boxes to cover buildings with vegetation, as this practice has been seen in many developed cities globally [24]. Green curtains and green facades have been used interchangeably in research studies. To create a green curtain, hanging shrubs are planted around the building as part of the facade [25]. Panels or geotextile felts are used to make living walls, either pre-cultivated or fixed to vertical supports or on the wall structure itself [25,26].

Vertical greenery systems have shown their advantages in different climates, as green walls improve the thermal comfort of indoor environments, and can also reduce a building's energy consumption during the summer and winter seasons [27–30]. Moreover, the cooling load was reduced by 20% when plants were used as green walls instead of blinds under the same solar radiation intensities [31]. In comparison to the concrete wall, Cheng [32] found that green walls can reduce indoor temperature and delay the heat transfer from outdoor to indoors, while, in comparison to bare walls, green walls lead to a 6.1 °C and 4 °C reduction in external wall temperature on sunny and cloudy days, respectively [33]. Some other studies about the benefits and uses of green walls were conducted in different climates: Mediterranean [34], Mediterranean continental [25], hot and dry Middle Eastern [35], humid subtropical [36], temperate [37], temperate oceanic [33], tropical [32], subtropical [28], and maritime [31]. Overall, greenery systems can reduce the wall and roof surface temperature, resulting in a reduction in heat transfer through building envelopes, which can be as high as 80–90% [38]. Moreover, the external vertical greening fully uses the building's structural surfaces, such as facades, roofs, windows, columns, and balconies, to grow green plants. The external vertical greenery systems in buildings can address problems such as the lack of biodiversity [39], urban drainage pressures [40], improving indoor thermal environmental conditions, and reducing cooling load [41,42]. It is clear from these studies that the vertical greening effect on a building can vary based on climates, plant species, and other factors.

Recent studies on the uses of vertical greening systems mostly focus on green walls and green roofs, the former having greater potential considering that the extent of the facade greening area can double the ground footprint of buildings in urban centers [43,44]. Indoor green walls or vertical greening systems in the form of indoor living walls, and vertical greening systems can affect the room's relative humidity, as shown by [45], who

monitored relative humidity and found that, near the living wall, higher relative humidity levels were experienced, increasing the overall relative humidity by 15%. This additional indoor relative humidity was identified as a potential criticality of living walls, as it may cause respiratory problems [46]. In Athens, Greece, an investigation of the absolute relative humidity of an area shaded by a deciduous tree and an unshaded area was undertaken [47]. It was found that the relative humidity measured in the shaded area was constantly higher than the unshaded area, clearly showing the effects of evaporated water from the trees. In dry environments, high relative humidity may be favorable; however, in already humid climates, this may cause discomfort [48]. Monitoring relative humidity and implementing a ventilation system may aid in achieving more comfort for occupants [45]. The main factors that influence energy usage and climate are: vegetation quality and quantity, leaf area index, vegetation species, substrate properties, air ventilation/infiltration rate of the building, façade properties, location and orientation of the building, and vegetation and local climate [48]. Other forms of indoor greening can be integrating plants as additional insulation layers. Another beneficial effect of indoor vertical greening is IAQ. Studies have found that indoor vertical greening systems can prove IAQ [49,50] by decreasing carbon dioxide concentration [50] and can ultimately lead to fewer medical issues arising from poor IAQ [51].

Mostly outdoor vertical greening systems have been discussed in literature focusing on issues such as the insulating effects of plants on facades (mostly outdoor), plants' evaporative cooling effects, and habitat creation for urban wildlife. This particular research work focuses on passive low-tech windows with an indoor vertical greening system used as internal shading devices to capture solar energy, redistribute natural light, and create psychological comfort for the inhabitants. This study aims to monitor a prototype for an indoor green curtain. The objective is to assess the potential of this shading typology as a means to improve thermal comfort and the IAQ in residential applications for warm temperate climates. The assessment relies on a performance comparison of thermal comfort parameters (air temperature and relative humidity) and air quality. The thermal comfort parameters are compared between three modules: the prototype, a base case without any shading device, and an external window blind module. The air quality is only compared between the prototype module and base case without any shading device.

2. Methodology

The methodology consists of first designing and then constructing three modules: the No Curtain (NC) module, the Green Curtain (GC) module, and the Window Blind (WB) module, as shown in Figure 1. The first module, NC was used as a control or reference. Indeed, the window was cleaned and kept without any shading system. This module acted as room area in a house that receives maximum sunlight and heats at a higher rate than other areas. The GC was the second module which was set up on a wooden counter in front of a glass window panel. The third module accommodated an external blind to fully shade the window from the outside. All three modules were separated by plywood walls, in the form of plywood box frames with a plexiglass sheet opposite to the window frames from the inside to enclose the modules in the form of a room environment, shown in Figure 1. This allowed the indoor environment of the different modules to be compared, and it showed whether GC had been effective in improving thermal comfort and air quality inside the module environments. Sensors were set up on the surfaces of the module ceilings to monitor the thermal comfort parameters and air quality. A customized sensor was built to monitor the indoor solar radiation intensity coming from outside.

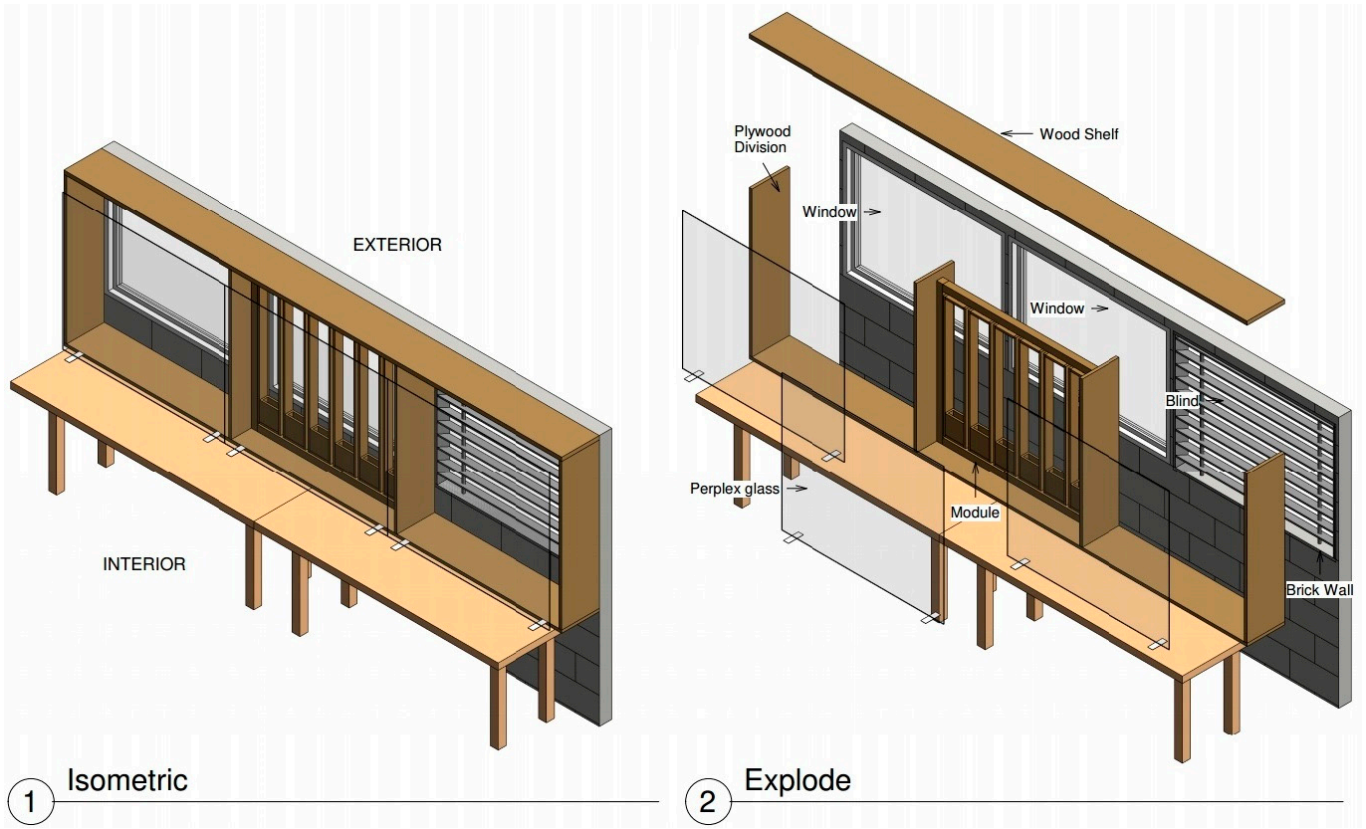

(**a**) (**b**)

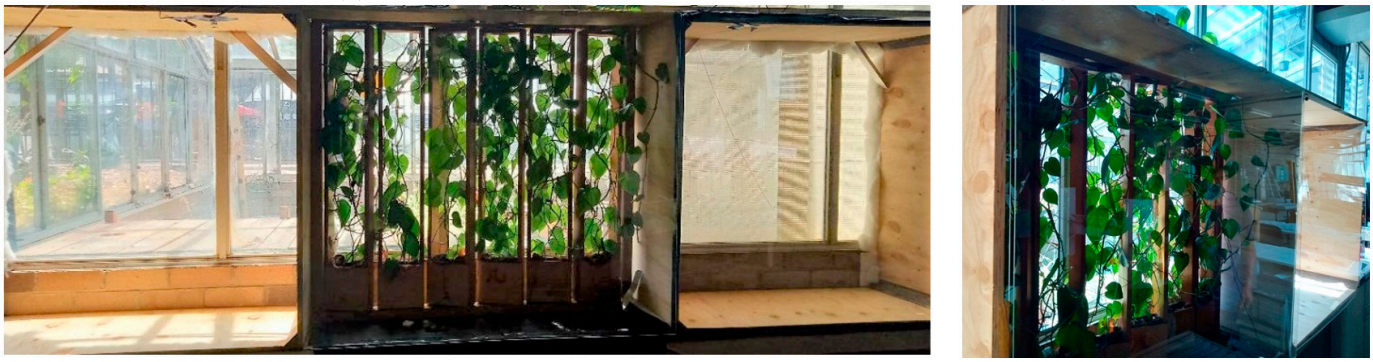

(**c**) (**d**)

Figure 1. (**a**) Isometric modeled image of the experimental set-up showing all the components, and exterior and interior environment. (**b**) Exploded view of the components of the experimental set-up. The model was designed and drafted in Autodesk Revit. (**c**) Experimental set-up showing three modules (NC, GC, and WB). Each section of the GC can be vertically rotated. The fully grown Philodendron cordatum plant is included on each section of the GC module. The hemp mesh running from top to bottom provided a climbing medium for the plant. (**d**) A 3D view of the plexiglass sheets in front of the modules. The external side of the modules is the glasshouse mimicking the Australian outback region climate. Detailed dimensions of the GC prototype and the experimental setup are shown in Appendix A (Figures A1 and A2).

2.1. Location and Climatic Conditions

The experimental site is located in Sydney, in the eastern part of New South Wales State, at 33.8688° S latitude and 151.2093° E longitude. Sydney has a warm temperate climate with four distinct seasons, shifting from mild and cool in the winter to warm and hot in the summer, with no extreme seasonal differences, as the weather is moderated by proximity to the ocean.

2.2. Experimental Set-up

The modules and the green curtain prototype were placed in an interior environment as shown in Figure 1a. The individual components in the experiment as modeled image are shown in Figure 1b. The exterior environment of the modules was a glasshouse. This choice allowed us to test the benefit of the green curtain in indoor module (room) conditions. Indeed, the glasshouse was not equipped with any shading system, and thus the indoor temperatures are usually higher than the ones normally found in residential buildings. The temperature in the glasshouse varied considerably, which ideally resembled the extreme climatic conditions of the Australian outback region; e.g., 50 °C temperature has also been recorded in the summer season. Therefore, the temperature in the controlled climate of the glasshouse was higher than the normal Sydney ambient temperature.

2.2.1. Design and Working Mechanism of Green Curtain Prototype

The entire curtain frame (Figure 1c,d) was made of commercial cedar also known as Western Red Cedar, treated to be water-resistant with natural sealants, such as Tung oil. The treatment included three to four coating layers of Tung oil, applied in 10 days. This sealant was chosen due to its environmental benefits; indeed, it is both biodegradable and renewable, making it an ideal material for this project [52]. Pivot hinges were used to hinge the panels from top and bottom. Indeed, the curtain is designed with a certain degree of flexibility, allowing the panels to rotate to either shade, and filter or allow sunlight in the room, according to the season's demand. The prototype is operated manually, and each panel can rotate 360°. This flexibility provides a higher degree of control to the occupants, which is proven to be beneficial in buildings [53]. A wooden ply box was made in the lower section of the panel (Figure 1c); it contains the soil and the plant in jute bags. For the connection between the parts of the prototype to support the plant's growth in an upward direction, an aluminum mesh was mounted, running from top to bottom. Plants took approximately three months to grow and climb the structure. For irrigation purposes, a pipe of 0.2 mm in diameter was provided at the bottom of the box to allow for the outflow of the water.

2.2.2. Plant Specie

For this experiment, Philodendron cordatum was chosen as the crawling plant (Figure 1c) due to its low maintenance cost. The Philodendron cordatum plant, also known as the Heart Leaf plant, is commonly used indoors, and it is renowned for its air-purifying qualities [54] by removing formaldehyde from the air. Moreover, it is a relatively tough plant, which makes it suitable for high-temperature applications. Soluble, all-purpose plant food was mixed with water and given to the plants weekly for faster growth, providing the plants with extra nutrients. The plants were placed in rectangular hessian bags before placing them in the panels. The bags were filled with peat moss. There was no irrigation system installed, and the plants were watered manually. Watering was carried out twice a week with a cup of water each time for each plant.

Hessian material was preferred for the plant bags because it is solely made from fibers of jute plants, making it fully biodegradable and organic. It is recyclable and reusable, making it an eco-friendly material and a sustainable alternative to plastic planter boxes. Compared to terracotta, the hessian fabric is lightweight yet durable, strong, and resilient, allowing the prototype to be easily portable and avoid adding any unnecessary extra weight.

2.2.3. Data Arrangements

The prototype was equipped with multiple sensors to detect air temperature, relative humidity, air quality, and solar radiation. The specifications of all the sensors are shown in Table 1. The air temperature and relative humidity sensors were placed just below the ceiling inside each module to allow for performance comparison. Figure 2 shows the location of the sensors. The solar radiation sensors were only used for the GC module

placed on both sides of the window glass near the ceiling, measuring the outside solar radiation intensity (q^r_{out}), and the radiation on the inner side of the window before the prototype, respectively, in W/m^2. It was noticed that there was negligible difference between the two, as the radiation on the inner side of the window was only 8% less than outside because the glass was highly transparent. Therefore, the radiation outside solar radiation was considered as the primary solar radiation value. The air quality sensors were only used for GC and WB modules measuring the quality of indoor air in μg/m^3. A preliminary test to compare the air quality of NC and WB was carried out for 48 h period where two sensors were arranged for the experiment. The results were monitored online, and it was found that the values in the two modules did not differ from each other. This result was expected since the primary factor of variation of air quality is the presence of plants in the GC module. Therefore, based on those 48 h data, we decided to install the air quality sensors only in GC and WB. Moreover, for comparison with GC, only one module was required as base case.

Table 1. Sensors and data-measuring period of the parameters.

Parameters	Duration of Measurement	Sensor	Measurement Range	Accuracy
Air temperature (°C) and relative humidity (%)	4 November 2021–22 March 2022	HOBO MX2302A	40–70 °C 0–100%	±0.2 °C ±2.5%
Solar radiation intensity (W/m^2)	15 December 2021–22 March 2022	Solar Jinie	0–1200 W/m^2	±20 W/m^2
Air quality (μg/m^3)	1 March 2022–21 March 2022	PM 2.5 Wireless Indoor, PM 2.5 Wireless Outdoor	0–999 μg/m^3	±15 μg/m^3

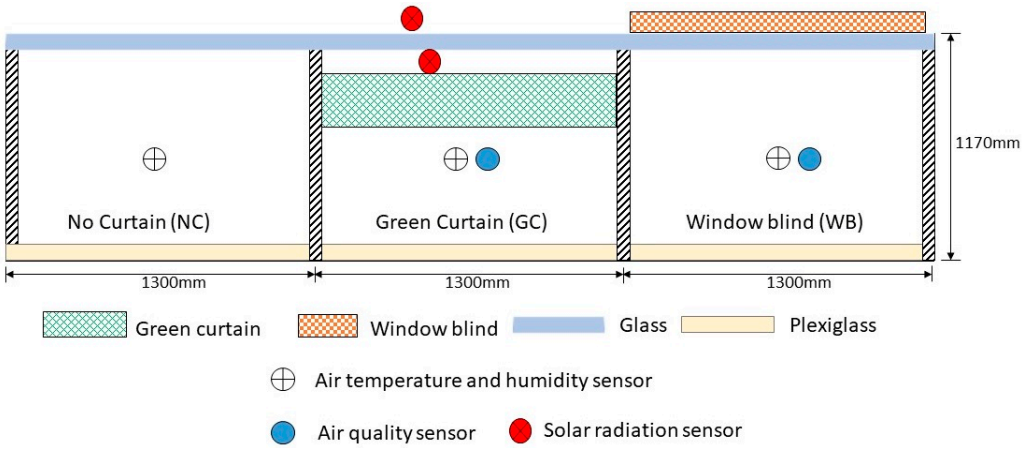

Figure 2. Experimental set-up showing three modules (NC, GC, and WB) and locations of all the sensors.

The air quality sensor was not installed in NC module because, during a litmus test before the actual measurement, it was noticed that the difference may not be a significant one. The sensor's specifications are shown in Table 1. Data gaps were fixed with linear interpolation.

3. Solar and Heat Energy Flow

The mechanisms of thermal transfer in the GC are convection (heat transport due to fluid motion), conduction (heat transfer due to molecular vibrations in a solid), and solar radiation (heat transport by photons). Part of the solar radiation is converted into heat and a part is biochemically stored by photosynthesis, and the remainder of the solar energy transmits through the plexiglass sheet. Part of the thermal energy is absorbed by the plants via evapotranspiration. The remaining thermal energy passes through the plexiglass sheet.

The heat flowing inside the building consists of an incoming solar radiation and a heat convection:

$$q_{Total} = q^r_{in} + q_{in} \quad (1)$$

where:

q_{Total} is the total energy;
q_{in} is the heat flowing by convective heat transfer;
q_{in}^{r} is the solar energy that passes through the plexiglass sheet (the last material layer in the GC module), which is given as

$$q_{in}^{r} = q_{out}^{r} - q_r - q_{ph} - q_h \quad (2)$$

where:

q_{out}^{r} is the incoming solar energy outside the GC module;
q_r is the solar energy reflected by the GC;
q_h is the solar energy converted into heat inside the GC module;
q_{ph} is the solar energy used by plant leaves for photosynthesis by the chemical reaction below [55]:

$$6CO_2 + 6H_2O \xrightarrow{q_{ph}} C_6H_{12}O_6 + 6O_2 \quad (3)$$

Photosynthesis absorbs only a part of the solar spectrum, usually around the 400–700 nm waveband that ranges from violet to red. Overall, the efficiency of photosynthesis varies depending on the specific plant species and environmental conditions, but it is generally in the range of 3–6% [56], and the percentage of absorption depends on many factors [57]. During photosynthesis, energy can be lost as heat due to the high temperature of the chloroplasts in which the process occurs. Additionally, energy can be lost through the dissipation of excess light energy, which can cause damage to the leaves. The radiation, q_h, accounts for all processes where the radiation is converted into heat. The reflection of solar energy by plants, q_r, is related to the albedo effect [58]. Albedo is a measure of the reflectivity of a surface, or the fraction of incident solar radiation that is reflected by the surface [59]. It is estimated that the reflectance of plants ranges from about 5% to 30%, depending on the wavelength of the incident radiation and the specific plant species [60].

Apart from radiation, we need to account for the heat flow through the GC module by convection and conduction in the various layers of materials of the module. It is assumed that the temperature variation on the GC is slow enough so that there is no accumulation of thermal energy by the thermal mass of the materials. The thermal gradient is calculated by $\Delta T = \frac{q}{R}$ in each solid phase, and $\Delta T = \frac{q}{h}$ in each gaseous phase. Here, R [Cm^2/W] is the R-value of the GC component and h [W/(Cm^2)] is the heat convection coefficient of the air. A special zone is the area occupied by the leaves. Here, there is a heat absorption Q [W/m^3] due to the combined effect of the evapotranspiration [61] and the fraction of solar radiation converted into heat.

$$Q = -Q_{et} + \frac{q_h}{D} \quad (4)$$

where:

Q_{et} [W/m^3] is the energy lost by evapotranspiration in the GC module;
q_h [W/m^2] is the solar energy converted into heat, also called solar irradiance;
D [m] is the thicknes of the folliage, $D = x_2 - x_1$.

The amount of energy required to evaporate water depends on several factors, including the initial temperature of the water, the atmospheric pressure, and the humidity of the air [62,63]. However, on average, it takes about 2257 kilojoules (kJ) of energy to evaporate one liter of water at room temperature and at standard atmospheric pressure [64]. This energy is used to overcome the intermolecular forces that hold the water molecules together, allowing them to break free and enter the gaseous phase. The power required to evaporate one liter of water in a day can be calculated as Power = Energy/Time = 2257 kJ/24 h = 94 W. Taking into account the fact that the average incoming solar radiation in the GC module is 50 W/m^2 × 1.3 m × 1.1 m = 70 W and the average amount of water added to the GC plant

is half a liter per day, the evapotranspiration (ET) will make a significant contribution to the energy budget.

The temperature profile in the folliage is calculated by the steady state heat equation

$$\frac{\mathrm{d}^2T}{\mathrm{d}x^2} = \frac{Q}{DR_{eff}} \tag{5}$$

where R_{eff} is the effective R-value of the foliage and D is the thickness of the foliage. Solving this equation leaves the parabolic temperature profile as shown in Figure 3. The integration constants can be solved using the heat fluxes as boundary conditions, i.e., temperature and heat fluxes are continuous at the boundaries.

$$T_{out} - T(x_1) = (\frac{1}{h_{out}} + \frac{1}{R_{glass}})q_{out} \tag{6}$$

where:

T_{out} is the outdoor temperature;
h_{out} is the convective heat transfer in the outside environment;
R_{glass} is the R-value of the window glass.

The boundary condition at the point x_2 is given by

$$T(x_2) - T_{in} = (\frac{1}{h_{in}} + \frac{1}{R_{plexi}})q_{in} \tag{7}$$

where:

T_{in} is the indoor temperature;
h_{in} is the convective heat transfer in the inside environment after the plexiglass sheet;
R_{plexi} is the R-value of the plexi glass.

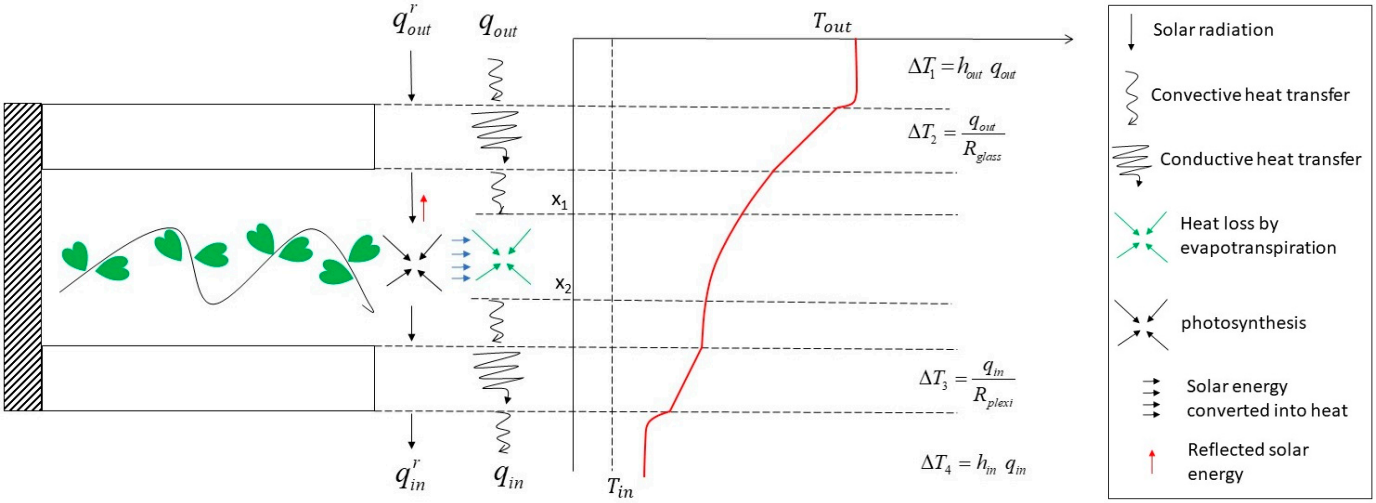

Figure 3. The mechanism of thermal transfer and heat absorption in the GC module. A part of the incoming solar radiation q_{out} [W/m^2] is absorbed by photosynthesis q_{ph} [W/m^2] (black arrows) and heat q_h [W/m^2] (blue arrows), and a part is reflected q_r [W/m^2] (red arrow). The remaining q_{in} enters the building. In addition, the interior heat flow q_{in} [W/m^2] is different than the exterior heat flow q_{out} [W/m^2] due to the amount of heat loss by evapotranspiration and the solar radiation converted into heat. The temperature profile is constructed based on the hypothesis of quasi-static equilibrium, and the temperature gradients are calculated based on thermal material parameters.

The governing equations show that the main effect of the evapotranspiration in the GC is to produce a drop of the heat flow indoors, $q_{in} = q_{out} - q_{et} + q_h$. In addition, the GC reduces the amount of solar radiation $q^r_{in} = q^r_{out} - q_r - q_{ph} - q_h$, allowing a comfortable

natural lighting indoors. Without CG, the indoor heat flow will be raised due to lack of evapotranspiration and the increase of indoor solar radiation. The main effect of the external blind is to drastically reduce the incoming solar radiation q_{out}, with a detrimental effect to the indoor natural illumination and creating discomfort for the indoor occupants.

4. Results and Analysis

The results are discussed in four sections. The first section discusses the ambient conditions in which the experiment was performed. The second section analyzes the solar radiation intensity and the air temperature during solar radiation hours. The third section then discusses the complete recorded temperature and relative humidity data (during solar and non-solar radiation hours). The last section discusses air quality. The temperature and relative humidity results are shown in the form of seasons: November was late spring, December was early summer, January was mid-summer, and February and March were late summer and early autumn, respectively.

4.1. Ambient Conditions

The experiment started in November 2021. It was the sixth wettest year on record, with 2021 rainfall being 30% above average. Sydney had its wettest November since national records began in 1900 [65]. It was not a hot summer. The external ambient mean hourly values with error bars of the outdoor temperature and relative humidity are shown in Figure 4.

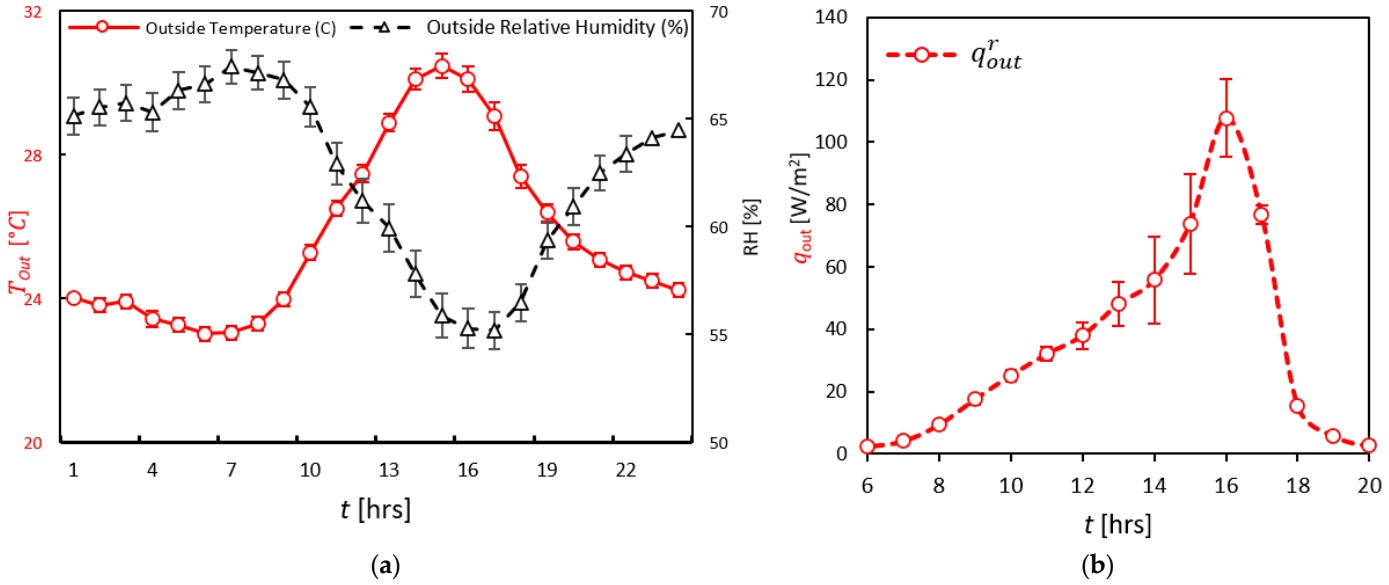

Figure 4. (**a**) Mean hourly outdoor temperature and relative humidity (with error bars) recorded during the experimental period (4 November 2021–21 March 2022). (**b**) Mean hourly solar radiation intensity (with error bars) in solar radiation hours recorded during the experimental period (8 October 2021–21 March 2022).

During the study period, the highest recorded temperature was 46.9 °C, with solar radiation hours ranging from 12 to 15. The study commenced in the spring of 2021 and concluded in the autumn of 2022. The observation period was 5 months (November, December, January, February, and March). During the experiment, the maximum temperatures were recorded around 15:00 hrs–16:00 hrs, while the minimum temperature was noticed in the early morning hours before the sunrise.

4.2. Solar Radiation and Air Temperature

The two external factors which had a high impact on the environment of the modules were the solar radiation (q^r_{out}) and the oudoor temperature T_{out}. As an example, the 1 February

data of solar radiation and temperatures are shown in Figure 5a,b, respectively. The raw data of every day for solar radiation and temperature are shown in the Supplementary Material. The daily solar radiation ranged up to 455 W/m^2 during the experiment. The mean value of solar radiation recorded was 38 W/m^2, though it kept increasing as the experiment moved into late summer (February) and early autumn (March). Due to the wet early and mid-summer, the solar radiation values were low because of a high proportion of diffuse radiation [66]. However, in late summer and early autumn, the intensity of solar radiation increased as the weather became clearer. The solar radiation was directly impacting the outdoor temperature, which was then affecting the temperature of the modules inside.

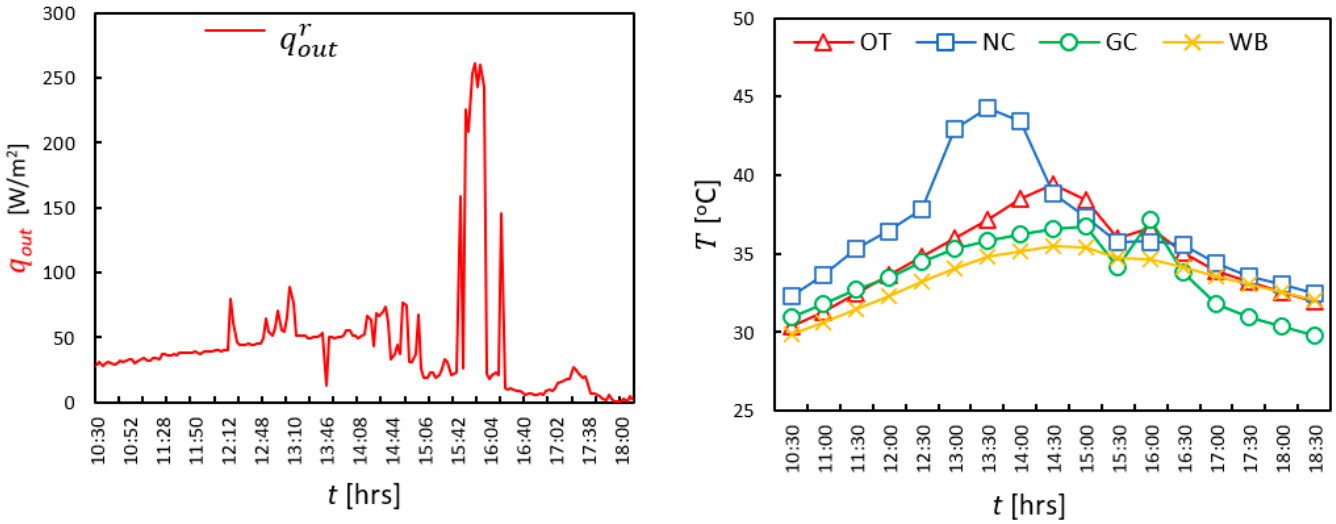

Figure 5. A typical presentation of the daily solar radiation and temperature measurements recorded during the experiment. (**a**) Solar radiation intensity recorded on 1 February 2022 externally. The data were recorded after every 2 min. (**b**) Temperature data of 1 February 2022 for the outdoor environment, and the inside of the three modules (NC, GC, and WB). The pattern shows three time frames: before the peak hours (10:30–12:30 hrs), at the peak hours (12:30–14:00 hrs), and after the peak hours (14:30–18:00 hrs). The time frames change on daily basis based on the solar angle.

Figure 5b shows the temperature recorded for every 30 min on 1 February during the solar radiation hours. The outdoor temperature is directly correlated to the solar radiation; e.g., from 18 January–22 January, 90% of the values of solar radiation were below 100 W/m^2 and the mean outdoor temperature during that period was 27 °C, which is 3 °C less than its mean temperature (30 °C) during January. It is important to note that Figure 6 shows a pattern of three different time frames: (i) the rise towards the peak temperature; (ii) the peak temperature hours; and (iii) the fall of temperature after the peak has passed. The peak hours graph kept on changing monthly; e.g., in November, the peak hours were between 13:30–15:00 hrs, in December 13:00–16:30 hrs, January 13:00–16:30 hrs, February 12:30–15:30 hrs, and March 12:00–15:00 hrs. High-temperature peaks were noticed in the NC module from late spring (November) to late summer (February). The primary peak (27.5 °C) occurred around 15:00 hrs in late spring (November) and slightly late in early summer (December) at 16:00 hrs (31 °C). However, a secondary peak (30 °C) was also noticed in early summer at around 13:30 hrs. In the mid-summer (January), two primary peaks were noticed at 13:30 hrs and 16:30 hrs, with temperatures of 33.5 °C each, respectively. During the peak hours, the GC always had a minimum value compared to the NC and was the quickest to cool when the peak was passed. It was primarily because of the evapotranspiration effect of the plants [67] in the GC module. This cooling-down effect after peak hours was also noticed in other studies [45,49,68]. The main reason that the peaks were found in the NC module the most was the entrapped heat being generated due

to the greenhouse effect [69]. As the WB was blocking most of the solar radiation, therefore, understandably, it had the minimum indoor temperature before and during the peak hours. However, due to some radiation still penetrating through the blinds, the entrapped heat inside the WB module increased the temperature.

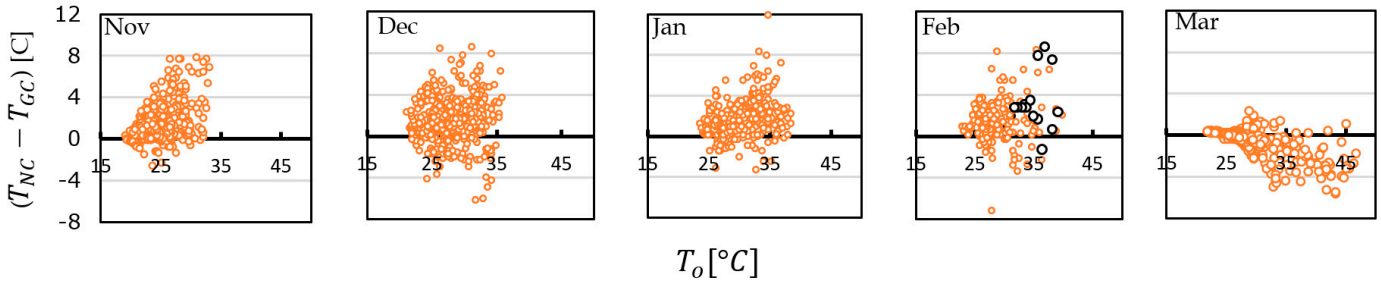

Figure 6. The difference between the temperature of NC and GC recorded during the peak solar radiation hours. The horizontal axis shows the outside temperature, and the vertical axis shows the difference of temperature between NC and GC. The black dots in late summer (February) corresponds to 1 February 2022 data points shown in Figure 5.

The absence of a plant delayed the cooling period in both the NC and WB blinds. As in the summer months (December, January, and February), the mean temperature in the after-peak hours (16:30–20:30 hrs) in GC was 1.5 ± 0.05 °C lesser than NC and 1 ± 0.05 °C than WB. This difference even reached up to 8 °C and 4 °C, respectively, on hotter days in particular hours. In early autumn (March), the change in the solar angle due to the seasonal variations resulted in high peaks noticed in the outside temperature.

The difference of air temperature between the base case module (NC) and GC, shown in Figure 6 during the peak solar radiation hours, clearly show the significance of a living plant medium. From late spring (November) to late summer (February), more than 90% of values were positive. In those positive values, more than 95% were between 0–4 °C. The maximum difference reached up to 11 °C in January. A temperature difference of 1–3 °C with an indoor plant medium was noticed in the indoor studies [70]. The seasonal shift in early autumn (Mar) shows more than 90% negative values. Though a short hot spell increased the outside temperature above 40 °C again and even up to 47 °C but the difference was in the negative, it was because, due to the change in the solar angle, the solar radiation was hitting the sensor probes in the GC module directly.

4.3. Temperature and Relative Humidity (during Solar and Non-Solar Radiation Hours)

From the box plot data shown in Figure 7, it is important to note that the mean value (x) and the median line are at the lowest in the GC module from late spring (November) to late summer (February). This shows the overall performance of the GC prototype to regulate the indoor temperature inside the module and keep it around or within the ASHRAE range. The evapotranspiration effect [67] of the GC causes this cooling effect inside the module. Moreover, on an average hourly basis, GC is 1.3 °C and 0.6 °C cooler than NC and WB, respectively. This can be verified by a meta-analysis study of green spaces [71]. WB had the lowest average maximum daily temperature, followed by GC and NC; this can be explained by the reflection of the solar radiation. However, some radiation still comes inside the WB and the heat then gets entrapped as with NC. Therefore, this entrapped heat in the form of high thermal mass [72] does not allow the WB and NC to get low quickly, compared to GC which had plants.

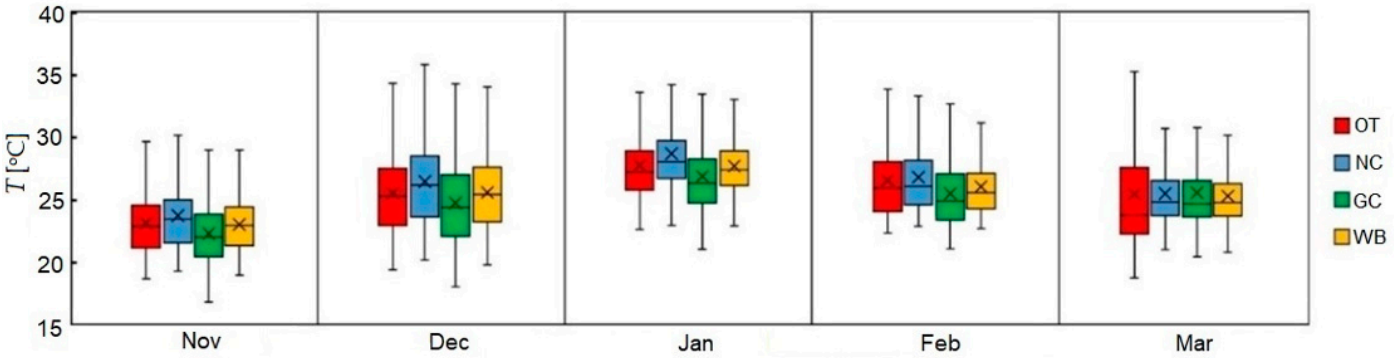

Figure 7. The complete recorded temperature data (solar and non-solar radiation hours) shown as box plots with error bars for outside temperature (OT) and the three modules (NC, GC, and WB) every month. The box plot shows a median (solid middle line), mean value (marker—(×)), the interquartile ranges (upper and lower limit lines of the boxes), and the range of maximum to minimum values (the whiskers), except for "outliers".

The maximum and minimum temperatures also ranged significantly within each season (Figure 7). It was important to note that the temperature range increased during the seasonal shifts; e.g., the largest temperature range overall was recorded in the NC module during late spring (November) (min = 23 °C, max = 45 °C), while the maximum in the GC was found in early autumn (March) between 20 °C (min) and 40 °C (max). The maximum variation in the outside temperature was found in March (min = 18 °C, max = 47 °C). The high temperatures of NC are due to entrapped heat between the window glass and the plexiglass sheet accumulated during the solar radiation hours of the day. The lack of ventilation and the trapping of the long wavelength radiation inside the NC caused a greenhouse effect [73].

The RH data are shown in Figure 8. GC had the highest RH in all the modules from late spring (November) till late summer (February). On a daily average basis, in late spring (November), the RH of GC was greater than OT, NC, and WB by 9%, 6%, and 7%, respectively. In the summer months (December, January, and February), this difference was 3.62%, 7.2%, and 5.72%. The high RH values of GC were due to transpiration, as the water travels from the root to the plant leaves, where it turns into water vapor and is released into the atmosphere [68]. Therefore, green plants can increase indoor relative humidity [74] and also regulate air temperature [75]. The minimum values were all recorded in the afternoon because the cooler morning air is closer to saturation than the hot afternoon air, even with the same amount of water vapor. The season shift from late summer to early autumn lowers the RH in GC and the difference is 1% approximately each between GC,NC and GC,WB. In March, the rise in RH values is due to the dip in the external and internal temperatures [76], as the weather becomes cooler, causing the air to be moist.

The maximum RH observed in GC was 93% on 23 December 2021, whereas the maximum outside RH was 94%, recorded in March. The average hourly peak was observed at 06:30 hrs. A regular pattern of a dip in relative humidity was seen in all modules from 09:00–15:30 hrs, because an increase in solar radiation decreases the vapor content in the air [77].

Practically, 98% of occupants are thermally satisfied when the temperature and relative humidity integration take place in the comfort zone suggested by ASHRAE Standard 55 [78]. Consequently, a person will feel almost exactly as cool at 24 °C and 60% relative humidity as at 26 °C and 30% relative humidity [36]. Moreover, the local standards of New South Wales (an Australian state) recommend a temperature of 20–26 °C [79]. Based on these standards, the frequencies of temperature and relative humidity are shown in Figure 9. It shows that the GC module had the maximum frequencies of temperatures falling between the recommended range for the occupants. The GC temperature complied with 66% of the acceptance limits of ASHRAE and NSW (20–26 °C), greater than WB (57%) and NC (51%).

In Figure 9, the frequencies of the relative humidities show that GC had the maximum frequencies falling between 70 to 80% compared to the other two modules.

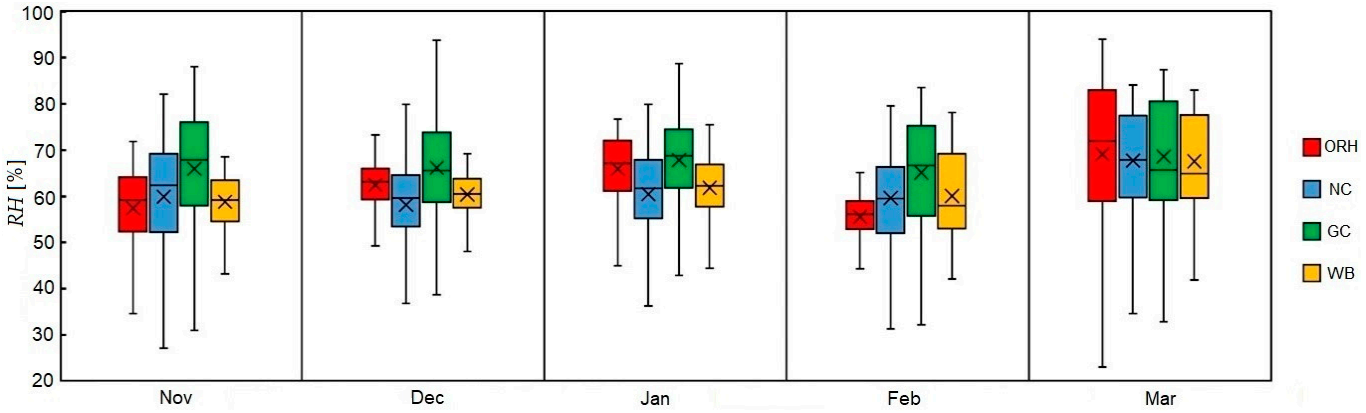

Figure 8. The complete recorded relative humidity data (solar and non-solar radiation hours) shown as box plots with error bars for outside temperature (OT) and inside the three modules (NC, GC, and WB) in every month. The box plot shows a median (solid middle line), mean value (marker—(×)), the interquartile ranges (upper and lower limit lines of the boxes), and the range of maximum to minimum values (the whiskers), except for "outliers".

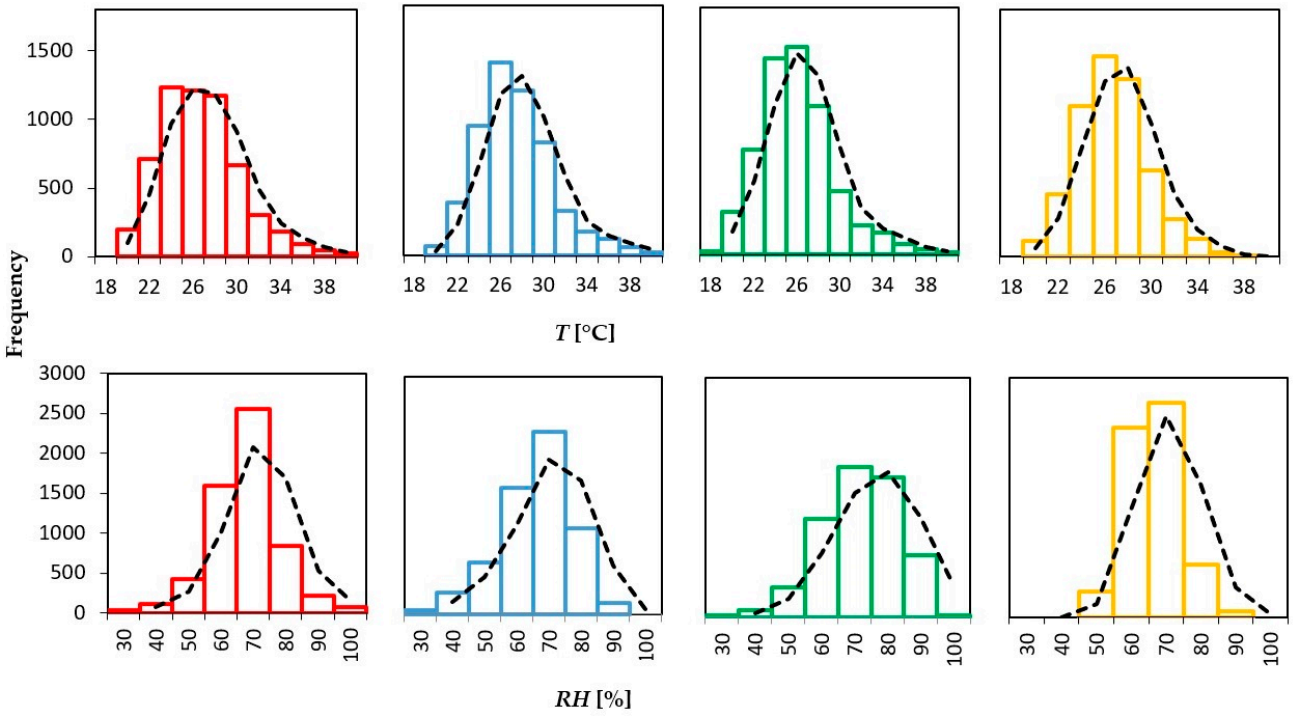

Figure 9. The frequencies of the temperature and relative huimidities inside the modules with moving average lines (black dotted) shown in black. The horizontal axis lines show a certain range of temperature and RH. The vertical axis line shows the frequency of occurrence of temperature and RH.

4.4. Air Quality

The air quality comparison between the GC and WB did not show a significant difference compared to each other, as shown in Figure 10. To examine the data of the Air Quality (AQ), the arithmetic theory of the null hypothesis was used [80], suggesting that no significant difference exists in the set of observed variables (GC-AQ and WB-AQ) between the two sets of observed data. The null hypothesis statement is that the difference in the mean of the AQ of the GC module is equal or not different from the mean of the

WB-AQ. The test was carried out for two time frames, 02:00–16:00 hrs and 16:00–02:00 hrs. It was found that, from 02:00–16:00 hrs, the *p*-value was 0.08 (>0.05), which means the null hypothesis was accepted, but, from 16:00–02:00 hrs, the *p* was 0.0001 (<0.05) and the null hypothesis was rejected. This means that, in the evening, the difference was significant and the GC module was more effective at decreasing the pollution compared to the WB module.

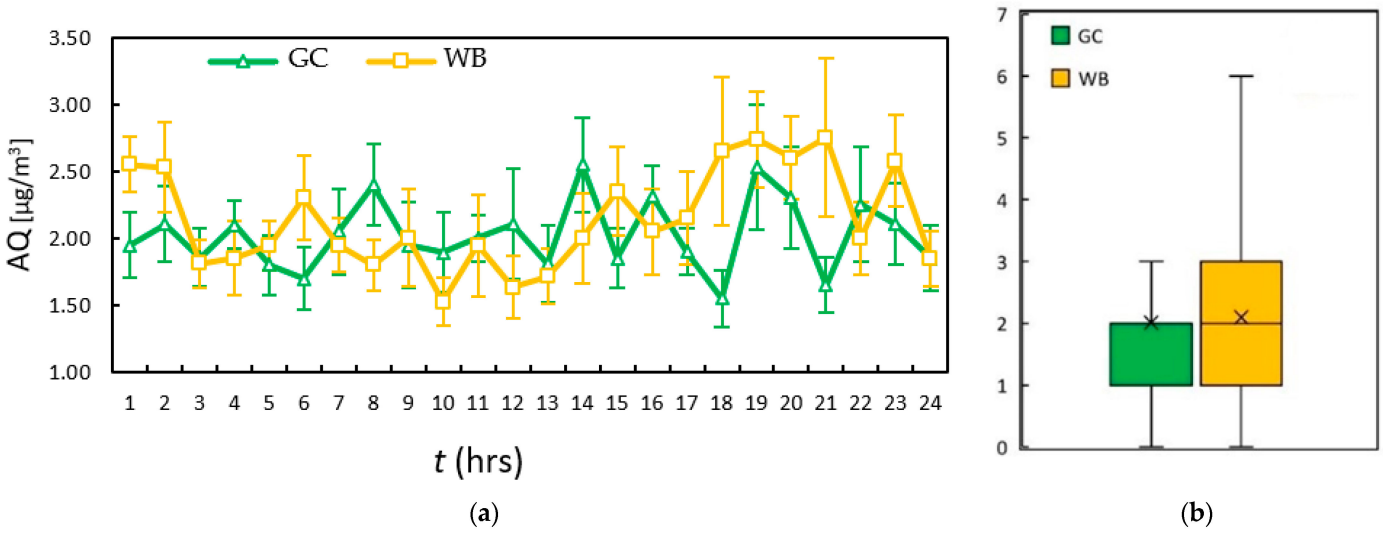

Figure 10. (**a**) Hourly mean data of AQ for GC and WB modules. The error bars were calcualted using standard error (SE); formula: SE = Standard Deviation/$\sqrt{}$ (sample size). These mean data were calculated from the complete raw data measured every 30 min from 1 March 2022 to 21 March 2022. (**b**) The box plot data distribution of the AQ data. The box plot shows median (solid middle line), mean marker (×) and the interquartile ranges; the whiskers give the range of maximum to minimum, except for "outliers".

Because of the lack of ventilation in both the modules, the air quality remained fairly constant in the range of healthy standards for air [81], except in the period between 1800 to 2200 hrs, when the AQ values increased in the module without GC, indicating higher pollution in the evening hours. The daily maximum, minimum and mean values of all the variables is shown in Table 2.

Table 2. Summary of the temperature, relative humidity, and air quality measured during the experimental period (solar + non-solar radiation hours). The standard errors are shown for the daily mean, maximum daily mean, and minimum daily mean. The daily mean was the average of all the values recorded for a variable. The maximum daily mean was found by finding the maximum value of a variable in 24 h and then finding the average of all those maximum values; the same applies for the minimum daily mean. The maximum and minimum values correspond to the highest and lowest values recorded for a variable during the whole data collection period.

	OT (°C)	NC (°C)	GC (°C)	WB (°C)	ORH (%)	NC (%)	GC (%)	WB (%)	GCAQ (µg/m³)	WBAQ (µg/m³)
Daily Mean	25.72 ± 0.22	26.39 ± 0.22	25.05 ± 0.20	25.64 ± 0.21	60.07 ± 1.30	60.74 ± 0.78	66.75 ± 0.77	61.43 ± 0.62	1.99 ± 0.09	2.19 ± 0.09
Max daily mean	31.30 ± 0.41	31.99 ± 0.42	30.39 ± 0.37	28.89 ± 0.29	65.37 ± 1.41	68.34 ± 0.67	77.09 ± 0.81	64.66 ± 0.62	0.87 ± 0.18	1.04 ± 0.22
Min daily mean	22.82 ± 0.21	23.90 ± 0.20	21.94 ± 0.18	23.55 ± 0.19	51.00 ± 1.35	46.94 ± 1.23	54.17 ± 1.02	57.08 ± 0.74	0.14 ± 0.03	0.13 ± 0.03
Max	46.90	44.85	39.99	36.72	0.00	94.00	84.12	93.78	9	11
Min	18.73	19.33	16.85	19.01	0.00	22.00	19.98	29.67	0	0

Overall, the plant (Philodendron cordatum) remained in good health, though some issues with the growth of the plant were anticipated, as Philodendron cordatum does not tolerate direct sunlight. However, it was found that the plant adapted relatively well to the solar radiation. Due to the lack of ventilation, in the last few weeks (in March) of the experiment, the number of brown (dead) leaves started to increase but, by then, the data collection process was completed. As the prototype potential difference was at

the maximum in the summer months, this indicated that it is a plant that requires less maintenance, that can adapt to harsh environmental conditions.

5. Conclusions

Vertical greening in form of green walls or living facades are used in buildings to improve air quality, reduce the urban heat island effect, provide habitat for wildlife, reduce noise pollution, and enhance the biophilic character of buildings. On the other hand, the indoor vertical greening system is less common and poorly investigated. This research is unique in developing an innovative indoor vertical greening in the form of a green curtain within an indoor setting of a prototype room. The green curtain provides to the occupants full control of the amount of sunlight that is allowed into the indoor environment based on the innovative rotating mechanism of its modules, allowing us to adjust the indoor natural light and the exposure of the plants to the required solar radiation needed for effective evapotranspiration. We demonstrated positive impacts on air temperature and air quality consistent with findings from outdoor greening studies. It was found that, during the peak solar radiation hours from late spring (November) to late summer (February), the difference between NC and GC air temperatures was mostly between 0–4 °C. On hotter days, during the peak hours, with regard to the maximum difference between NC, GC, and WB, GC was as high as 8 °C and 4 °C, respectively. In the after-peak hours, during the summer months, the GC module was cooler than the NC and WB modules by 1 °C and 1.5 °C, respectively. Overall, the GC created a climate in an intermediate space of the module that was characterized by lower temperature, heat absorption, higher humidity, and improved air quality in the evening hours. While the GC would not significantly affect the temperature/humidity indoors, it produces a significant reduction of the heat flow in the building envelope due to the combined effect of evapotranspiration, reflected solar radiation, and photosynthesis.

The implication of the initial findings is vast, as a simple indoor solution without any retrofitting requirement or an alternative to an energy-saving retrofit strategy for windows provides a feasible option to mitigate heat gain. Moreover, we optimized two main thermal comfort factors, air temperature and relative humidity, in the desired range, that improve thermal comfort. In addition, the design adopted a biophilic design approach that creates a natural indoor environment, providing the benefits of biophilia by bringing the green outdoors indoors. High humidity levels were observed near the living wall due to plant evapotranspiration, which is beneficial in the case of dry indoor environments.

5.1. Direction for Future Studies and Methodological Recommendations

The future developments of the research will aim to investigate the performance and benefits of the GC when applied to realistic settings in the form of larger module areas. As for a more real-world setting, proper ventilation is advised to avoid problems associated with excessive moisture because there was reduced air circulation from outside to inside or vice versa. The model can also be studied for naturally ventilated buildings, where more air circulation effects on the plant growth and comfort parameters can be studied. The prototype should also be tested in other seasons, e.g., in winter or early spring. To investigate the fluctuations of the indoor operative temperature over the entire year under various indoor air temperature set-points, a computer simulation model can be developed using a BIM (building information modeling) tool, e.g., Integrated Environmental Solutions [82] or Energy Plus [83]. Computer simulations should account for the thermal mass effect as observed in the experiments reported here. Moreover, a numerical model assessment of the GC prototype is recommended for future studies to evaluate the behavior of the prototype when upscaled. It is important to arrange all the necessary equipment for measuring all the variables, e.g., evapotranspiration rate, photosynthetic rate, latent heat of vaporization, short/long incident/reflected solar radiation, and temperature sensors, inside the leaves of the GC. Moreover, multiple sensors for each variable should be used to improve indoor environmental quality management [84].

However, the design of the prototype for every plant may be different, depending on the plant species' growth rate and shape; e.g., some plant species grow from top to bottom, others sideways. To further improve the prototype design, we should minimize human interaction by integrating it with BEMS (Building Energy Management Systems). Moreover, some other benefits of plants should be studied, e.g., carbon reduction from a building performance point of view, and numerous health and well-being, psychological, cognitive, and behavioral benefits from the human performance point of view. All the recommendations can assist in promoting an affordable and biophilic solution to improve indoor environmental quality (IEQ).

5.2. Limitations

This study was not benchmarked with other studies because no rotating-mechanism-based indoor plant was found in the literature. However, in the future, this study can be considered as a benchmark of calibration for other plants. Some consideration can also be given to adverse plant-related effects because those effects have received very little or no attention from built-environment-focused studies.

Human habitation in cities occurs in indoor environments and this study has provided an opportunity to enhance building occupant health, well-being, and comfort. This research further identifies the need for future research to consider and integrate plant science aspects, providing a foundation for the inclusion of indoor living walls in urban built environments.

Supplementary Materials: The following supporting information can be downloaded at: https://www.mdpi.com/article/10.3390/buildings13051307/s1. Figure S1: Daily pattern of solar radiation intensity during the solar radiation hours from 8 December 2021–22 March 2022. The redline shows the outside solar radiation intensity measured by the sensor installed outside and the green line shows the radiation that passes through the window glass. The flat line from 22–27 December (2021), shows the data was not recorded. Figure S2: Daily pattern of temperatures recorded outside, and in the three modules (NC, GC, WB). The pattern shows three-time frames; before the peak hours, at the peak hours, and after the peak hours. The time frames have changed on daily basis based on the solar angle. Figure S3: Complete Relative humidity profile pattern recorded every 30 mins for outside environment and in the three modules (NC, GC, and WB). This measurement is from 4 November 2021 to 21 March 2022.

Author Contributions: The author contribution is as follows: conceptualization, N.W. and F.A.-M.; methodology, G.Q. and A.B.; validation, G.Q., F.A.-M. and A.B.; formal analysis, G.Q.; investigation, G.Q.; data curation, G.Q.; writing—original draft preparation, G.Q.; writing—review and editing, G.Q., F.A.-M. and A.B.; visualization, G.Q., F.A.-M. and A.B.; supervision, F.A.-M. and A.B.; project administration, F.A.-M. and G.Q. All authors have read and agreed to the published version of the manuscript.

Funding: This research received no external funding.

Data Availability Statement: Data is available on request.

Acknowledgments: The authors express appreciation to Rahmee Chowdhury, Gaurav Poddar, and Janane Yogesan for assisting in the CAD model of the prototype. The authors also thank Theo Gresley-Daines (The University of Sydney) for building the GC prototype.

Conflicts of Interest: All authors have seen and approved the final version of the manuscript being submitted. They warrant that the article is the author's original work, has not received prior publication, and is not under consideration for publication elsewhere.

Appendix A Green Curtain Prototype Experiment Components

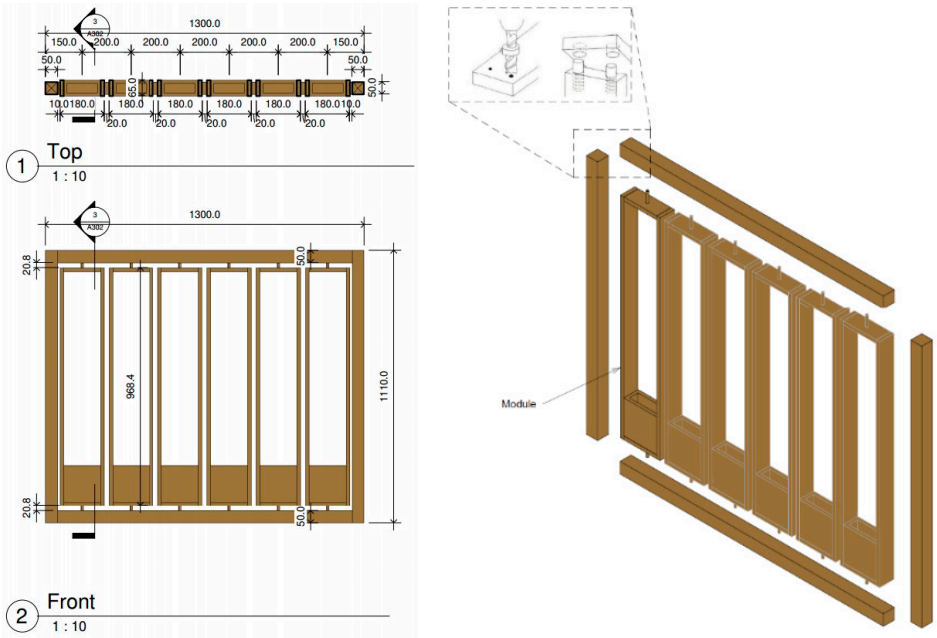

Figure A1. Front view and isometric 3D modeled view of all the components of the green curtain prototype. All units in mm.

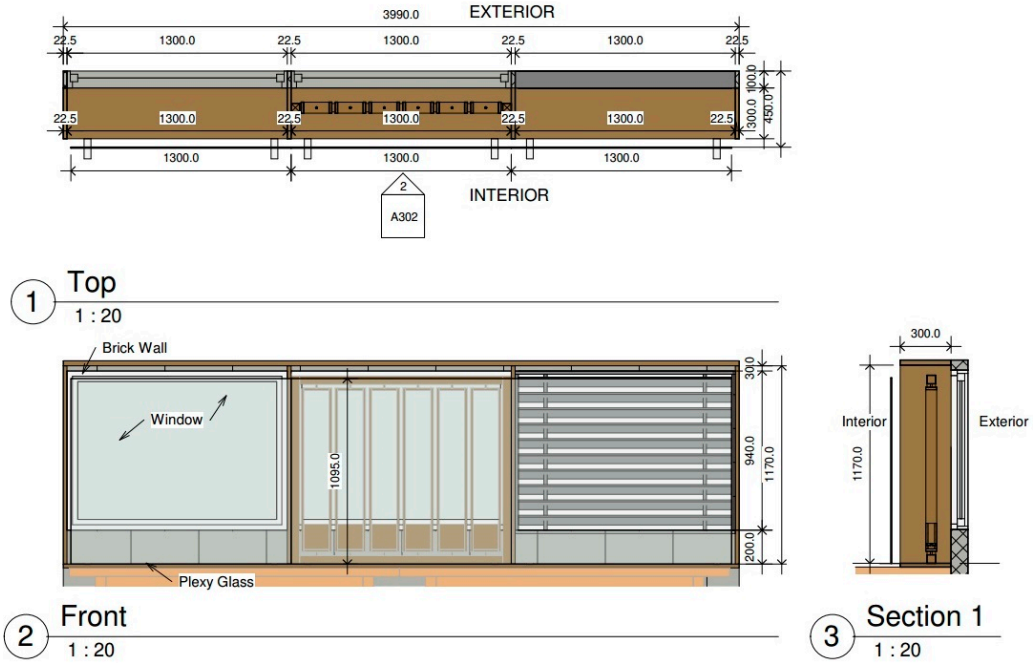

Figure A2. Section and top view of all the components of the experimental set-up. All units in mm.

References

1. Kaloustian, N.; Diab, Y. Effects of urbanization on the urban heat island in Beirut. *Urban Clim.* **2015**, *14*, 154–165. [CrossRef]
2. Wang, S.; Gao, S.; Li, S.; Feng, K. Strategizing the relation between urbanization and air pollution: Empirical evidence from global countries. *J. Clean. Prod.* **2020**, *243*, 118615. [CrossRef]
3. Tam, B.Y.; Gough, W.A.; Mohsin, T. The impact of urbanization and the urban heat island effect on day to day temperature variation. *Urban Clim.* **2015**, *12*, 1–10. [CrossRef]
4. Arfanuzzaman, M.; Rahman, A.A. Sustainable water demand management in the face of rapid urbanization and ground water depletion for social–ecological resilience building. *Glob. Ecol. Conserv.* **2017**, *10*, 9–22. [CrossRef]

5. Miller, J.D.; Hutchins, M. The impacts of urbanisation and climate change on urban flooding and urban water quality: A review of the evidence concerning the United Kingdom. *J. Hydrol. Reg. Stud.* **2017**, *12*, 345–362. [CrossRef]
6. Cao, X.; Dai, X.; Liu, J. Building energy-consumption status worldwide and the state-of-the-art technologies for zero-energy buildings during the past decade. *Energy Build.* **2016**, *128*, 198–213. [CrossRef]
7. Huang, M.; Hao, X.; Li, C. Heat and Mass Transfer of Evaporative Wall and Its Cooling Load Calculation. *Procedia Eng.* **2017**, *205*, 2762–2770. [CrossRef]
8. Cetin, K.S.; Fathollahzadeh, M.H.; Kunwar, N.; Do, H.; Tabares-Velasco, P.C. Development and validation of an HVAC on/off controller in EnergyPlus for energy simulation of residential and small commercial buildings. *Energy Build.* **2019**, *183*, 467–483. [CrossRef]
9. Spiru, P.; Simona, P.L. A review on interactions between energy performance of the buildings, outdoor air pollution and the indoor air quality. *Energy Procedia* **2017**, *128*, 179–186. [CrossRef]
10. (EAP) USEPA. *Introduction to Indoor Air Quality United States*; EPA: Washington, DC, USA, 2020. Available online: https://www.epa.gov/indoor-air-quality-iaq/introduction-indoor-air-quality#:~:text=Inadequate%20ventilation%20can%20increase%20indoor,increase%20concentrations%20of%20some%20pollutants (accessed on 6 March 2022).
11. ASHRAE. *Indoor Air Quality (IAQ)*; American Society of Heating, Refrigerating and Air-Conditioning Engineers: Atlanta, GA, USA, 2020. Available online: https://xp20.ashrae.org/terminology/index.php?term=indoor%20air%20quality%20(IAQ) (accessed on 5 April 2022).
12. (Institute) IIWB. The Value of WELL 2014. Available online: https://www.wellcertified.com/certification/v1/ (accessed on 10 January 2021).
13. (Council) UUSgb. Green Building 101: What Is Indoor Environmental Quality? *2014*. Available online: https://www.usgbc.org/articles/green-building-101-what-indoor-environmental-quality (accessed on 15 December 2021).
14. Al horr, Y.; Arif, M.; Katafygiotou, M.; Mazroei, A.; Kaushik, A.; Elsarrag, E. Impact of indoor environmental quality on occupant well-being and comfort: A review of the literature. *Int. J. Sustain. Built Environ.* **2016**, *5*, 1–11. [CrossRef]
15. Zhong, W.; Schröder, T.; Bekkering, J. Biophilic design in architecture and its contributions to health, well-being, and sustainability: A critical review. *Front. Archit. Res.* **2022**, *11*, 114–141. [CrossRef]
16. Reed, R.G.; Wilkinson, S.J. The increasing importance of sustainability for building ownership. *J. Corp. Real Estate* **2005**, *7*, 339–350. [CrossRef]
17. Al Horr, Y.; Arif, M.; Kaushik, A.; Mazroei, A.; Elsarrag, E.; Mishra, S. Occupant productivity and indoor environment quality: A case of GSAS. *Int. J. Sustain. Built Environ.* **2017**, *6*, 476–490. [CrossRef]
18. ASHRAE. *Indoor Environmental Quality (IEQ)*; ASHRAE: Atlanta, GA, USA, 2020. Available online: https://xp20.ashrae.org/terminology/index.php?term=indoor%20environment%20quality%20(IEQ)#:~:text=)%22%20Back%20%7C%20Next-,indoor%20environment%20quality%20(IEQ),%2C%20healthy%2C%20and%20comfortable%20buildings (accessed on 27 November 2022).
19. Bratman, G.N.; Daily, G.C.; Levy, B.J.; Gross, J.J. The benefits of nature experience: Improved affect and cognition. *Landsc. Urban Plan.* **2015**, *138*, 41–50. [CrossRef]
20. Europe WROf. *Urban Green Spaces and Health—A Review of Evidence*; WHO (World Health Organization): Copenhagen, Denmark, 2016.
21. Tyrväinen, L.; Ojala, A.; Korpela, K.; Lanki, T.; Tsunetsugu, Y.; Kagawa, T. The influence of urban green environments on stress relief measures: A field experiment. *J. Environ. Psychol.* **2014**, *38*, 1–9. [CrossRef]
22. Li, F.; Zheng, W.; Wang, Y.; Liang, J.; Xie, S.; Guo, S.; Li, X.; Yu, C. Urban Green Space Fragmentation and Urbanization: A Spatiotemporal Perspective. *Forests* **2019**, *10*, 333. [CrossRef]
23. Darlington, A. *Ecology of Walls*; Heinemann Educational Books: London, UK, 1981.
24. Wilkinson, S.; Brown, P.; Ghosh, S. Expanding the living architecture in Australia. Green Cities. 2018. Available online: https://www.horticulture.com.au/growers/help-your-business-grow/research-reports-publications-fact-sheets-and-more/gc15001/ (accessed on 6 March 2022).
25. Pérez, G.; Rincón, L.; Vila, A.; González, J.M.; Cabeza, L.F. Green vertical systems for buildings as passive systems for energy savings. *Appl. Energy* **2011**, *88*, 4854–4859. [CrossRef]
26. Jim, C.Y. Greenwall classification and critical design-management assessments. *Ecol. Eng.* **2015**, *77*, 348–362. [CrossRef]
27. Ip, K.; Lam, M.; Miller, A. Shading performance of a vertical deciduous climbing plant canopy. *Build. Environ.* **2010**, *45*, 81–88. [CrossRef]
28. Wong, I.; Baldwin, A.N. Investigating the potential of applying vertical green walls to high-rise residential buildings for energy-saving in sub-tropical region. *Build. Environ.* **2016**, *97*, 34–39. [CrossRef]
29. Feitosa, R.C.; Wilkinson, S. Retrofitted green roofs and walls and improvements in thermal comfort. *AIP Conf. Proc.* **2017**, *1856*, 020006.
30. Castiglia Feitosa, R.; Wilkinson, S.J.; Oliveira, B.; Hacon, S. Wind and greenery effects in attenuating heat stress: A case study. *J. Clean. Prod.* **2021**, *291*, 125919. [CrossRef]
31. Stec, W.J.; van Paassen, A.H.C.; Maziarz, A. Modelling the double skin façade with plants. *Energy Build.* **2005**, *37*, 419–427. [CrossRef]
32. Cheng, C.Y.; Cheung, K.K.S.; Chu, L.M. Thermal performance of a vegetated cladding system on facade walls. *Build. Environ.* **2010**, *45*, 1779–1787. [CrossRef]

33. Cuce, E. Thermal regulation impact of green walls: An experimental and numerical investigation. *Appl. Energy* **2017**, *194*, 247–254. [CrossRef]
34. Akbari, H.; Kurn, D.M.; Bretz, S.E.; Hanford, J.W. Peak power and cooling energy savings of shade trees. *Energy Build.* **1997**, *25*, 139–148. [CrossRef]
35. Haggag, M.; Hassan, A.; Qadir, G. Energy and Economic Performance of Plant-Shaded Building Façade in Hot Arid Climate. *Sustainability* **2017**, *9*, 2026. [CrossRef]
36. Bianco, L.; Serra, V.; Larcher, F.; Perino, M. Thermal behaviour assessment of a novel vertical greenery module system: First results of a long-term monitoring campaign in an outdoor test cell. *Energy Effic.* **2017**, *10*, 625–638. [CrossRef]
37. Scarpa, M.; Mazzali, U.; Peron, F. Modeling the energy performance of living walls: Validation against field measurements in temperate climate. *Energy Build.* **2014**, *79*, 155–163. [CrossRef]
38. Seyam, S. The impact of greenery systems on building energy: Systematic review. *J. Build. Eng.* **2019**, *26*, 100887. [CrossRef]
39. Mayrand, F.; Clergeau, P.; Vergnes, A.; Madre, F. Chapter 3.13–Vertical Greening Systems as Habitat for Biodiversity. In *Nature Based Strategies for Urban and Building Sustainability*; Pérez, G., Perini, K., Eds.; Butterworth-Heinemann: Oxford, UK, 2018; pp. 227–237.
40. Perini, K.; Rosasco, P. Is greening the building envelope economically sustainable? An analysis to evaluate the advantages of economy of scope of vertical greening systems and green roofs. *Urban For. Urban Green.* **2016**, *20*, 328–337. [CrossRef]
41. Hoyano, A. Climatological uses of plants for solar control and the effects on the thermal environment of a building. *Energy Build.* **1988**, *11*, 181–199. [CrossRef]
42. Mathew, A.; Khandelwal, S.; Kaul, N. Investigating spatial and seasonal variations of urban heat island effect over Jaipur city and its relationship with vegetation, urbanization and elevation parameters. *Sustain. Cities Soc.* **2017**, *35*, 157–177. [CrossRef]
43. Jim, C.Y. Thermal performance of climber greenwalls: Effects of solar irradiance and orientation. *Appl. Energy* **2015**, *154*, 631–643. [CrossRef]
44. He, Y.; Yu, H.; Ozaki, A.; Dong, N.; Zheng, S. An investigation on the thermal and energy performance of living wall system in Shanghai area. *Energy Build.* **2017**, *140*, 324–335. [CrossRef]
45. Fernández-Cañero, R.; Urrestarazu, L.P.; Franco Salas, A. Assessment of the Cooling Potential of an Indoor Living Wall using Different Substrates in a Warm Climate. *Indoor Built Environ.* **2011**, *21*, 642–650. [CrossRef]
46. Baughman, A.; Arens, E. Indoor humidity and human health–Part I: Literature review of health effects of humidity-influenced indoor pollutants. *ASHRAE Trans.* **1996**, *102*, 193–211.
47. Papadakis, G.; Tsamis, P.; Kyritsis, S. An experimental investigation of the effect of shading with plants for solar control of buildings. *Energy Build.* **2001**, *33*, 831–836. [CrossRef]
48. Wang, Y.; Bakker, F.; de Groot, R.; Wörtche, H. Effect of ecosystem services provided by urban green infrastructure on indoor environment: A literature review. *Build. Environ.* **2014**, *77*, 88–100. [CrossRef]
49. Moya, T.A.; van den Dobbelsteen, A.; Ottele, M.; Bluyssen, P.M. A review of green systems within the indoor environment. *Indoor Built Environ.* **2019**, *28*, 298–309. [CrossRef]
50. Cetin, M.; Sevik, H. Measuring the Impact of Selected Plants on Indoor CO_2 Concentrations. *Pol. J. Environ. Stud.* **2016**, *25*. [CrossRef] [PubMed]
51. Jones, A.P. Indoor air quality and health. *Atmos. Environ.* **1999**, *33*, 4535–4564. [CrossRef]
52. Ramage, M.; Burridge, H.; Wicher, M.; Fereday, G.; Reynolds, T.; Shah, D.; Wu, G.; Yu, L.; Fleming, P.; Densley-Tingley, D.; et al. The wood from the trees: The use of timber in construction. *Renew. Sustain. Energy Rev.* **2017**, *68*, 333–359. [CrossRef]
53. Kwon, M.; Remøy, H.; van den Dobbelsteen, A.; Knaack, U. Personal control and environmental user satisfaction in office buildings: Results of case studies in the Netherlands. *Build. Environ.* **2019**, *149*, 428–435. [CrossRef]
54. Today, P.C. Growing Heartleaf Philodendron: Philodendron Cordatum Care 2019. Available online: https://plantcaretoday.com/philodendron-cordatum.html (accessed on 10 December 2021).
55. Katul, G.G.; Oren, R.; Manzoni, S.; Higgins, C.; Parlange, M.B. Evapotranspiration: A process driving mass transport and energy exchange in the soil-plant-atmosphere-climate system. *Rev. Geophys.* **2012**, *50*. [CrossRef]
56. Zipfel, C.; Robatzek, S. Pathogen-associated molecular pattern-triggered immunity: Veni, vidi . . . ? *Plant Physiol.* **2010**, *154*, 551–554. [CrossRef]
57. Monteith, J. Solar radiation and productivity in tropical ecosystems. *J. Appl. Ecol.* **1972**, *9*, 747–766. [CrossRef]
58. Hussain, C.M. *Handbook of Environmental Materials Management*; Springer: Cham, Switzerland, 2019.
59. Kiehl, J.T.; Trenberth, K.E. Earth's Annual Global Mean Energy Budget. *Bull. Am. Meteorol. Soc.* **1997**, *78*, 197–208. [CrossRef]
60. Gates, D.M. Leaf Temperature and Transpiration1. *Agron. J.* **1964**, *56*, 273–277. [CrossRef]
61. Zhang, L.; Deng, Z.; Liang, L.; Zhang, Y.; Meng, Q.; Wang, J.; Santamouris, M. Thermal behavior of a vertical green facade and its impact on the indoor and outdoor thermal environment. *Energy Build.* **2019**, *204*, 109502. [CrossRef]
62. Hargreaves, G.H.; Samani, Z.A. Reference crop evapotranspiration from temperature. *Appl. Eng. Agric.* **1985**, *1*, 96–99. [CrossRef]
63. Hipps, L.E.; Asrar, G.; Kanemasu, E.T. Assessing the interception of photosynthetically active radiation in winter wheat. *Agric. Meteorol.* **1983**, *28*, 253–259. [CrossRef]
64. Lide, D.R. *The CRC Handbook of Chemistry and Physics*, 85th ed.; CRC Press: Boca Raton, FL, USA, 2004.
65. Australia BoM. New South Wales in 2021: Very Wet Overall and Relatively Cool 2021. Available online: http://www.bom.gov.au/climate/current/annual/nsw/summary.shtml (accessed on 5 May 2022).

66. Page, J. Chapter IIA-1–The Role of Solar-Radiation Climatology in the Design of Photovoltaic Systems. In *Practical Handbook of Photovoltaics*, 2nd ed.; McEvoy, A., Markvart, T., Castañer, L., Eds.; Academic Press: Boston, MA, USA, 2012; pp. 573–643.
67. Groh, J.; Pütz, T.; Gerke, H.H.; Vanderborght, J.; Vereecken, H. Quantification and Prediction of Nighttime Evapotranspiration for Two Distinct Grassland Ecosystems. *Water Resour. Res.* **2019**, *55*, 2961–2975. [CrossRef]
68. Deng, L.; Deng, Q. The basic roles of indoor plants in human health and comfort. *Environ. Sci. Pollut. Res.* **2018**, *25*, 36087–36101. [CrossRef]
69. Jain, P.C. Greenhouse effect and climate change: Scientific basis and overview. *Renew. Energy* **1993**, *3*, 403–420. [CrossRef]
70. Abdo, P.; Huynh, B.P. An experimental investigation of green wall bio-filter towards air temperature and humidity variation. *J. Build. Eng.* **2021**, *39*, 102244. [CrossRef]
71. Bowler, D.E.; Buyung-Ali, L.; Knight, T.M.; Pullin, A.S. Urban greening to cool towns and cities: A systematic review of the empirical evidence. *Landsc. Urban Plan.* **2010**, *97*, 147–155. [CrossRef]
72. Dunster, B.; Simmons, C.; Gilbert, B. *Thermal Mass*; Taylor & Francis: London, UK, 2021; pp. 185–186.
73. Kweku, D.W.; Bismark, O.; Maxwell, A.; Desmond, K.A.; Danso, K.B.; Oti-Mensah, E.A.; Quachie, A.T.; Adormaa, B.B. Greenhouse effect: Greenhouse gases and their impact on global warming. *J. Sci. Res. Rep.* **2018**, *17*, 1–9. [CrossRef]
74. Salt, D.E.; Blaylock, M.; Kumar, N.P.; Dushenkov, V.; Ensley, B.D.; Chet, I.; Raskin, I. Phytoremediation: A novel strategy for the removal of toxic metals from the environment using plants. *Bio/Technology* **1995**, *13*, 468–474. [CrossRef]
75. Liu, F.; Yan, L.; Meng, X.; Zhang, C. A review on indoor green plants employed to improve indoor environment. *J. Build. Eng.* **2022**, *53*, 104542. [CrossRef]
76. Hyndman, B. Chapter 91–Heating, ventilation, and air conditioning. In *Clinical Engineering Handbook*, 2nd ed.; Iadanza, E., Ed.; Academic Press: Cambridge, MA, USA, 2020; pp. 662–666.
77. Lightfoot, H. Earth's Temperature Versus the Sun, Water Vapor and CO_2. *J. Basic Appl. Sci.* **2021**, *17*, 44–53. [CrossRef]
78. American National Standards Institute. *Thermal Environmental Conditions for Human Occupancy*; American Society of Heating, Refrigerating and Air-Conditioning Engineers: Atlanta, GA, USA, 2004.
79. NSW. Maintaining Thermal Comfort in Indoor Work Environments: Safework NSW. 2022. Available online: https://www.safework.nsw.gov.au/resource-library/heat-and-environment/maintaining-thermal-comfort-in-indoor-work-environments (accessed on 22 February 2022).
80. Anderson, D.R.; Burnham, K.P.; Thompson, W.L. Null hypothesis testing: Problems, prevalence, and an alternative. *J. Wildl. Manag.* **2000**, *64*, 912–923. [CrossRef]
81. (EPA) Epa. *Revised Air Quality Standards for Particle Pollution and Updates to the Air Quality Index (aqi). The National Ambient Air Quality Standards for Particle Pollution*; EPA: Washington, DC, USA, 2012.
82. Solutions, I.E. Help Manual 2019. Available online: https://help.iesve.com/ve2019/ (accessed on 21 September 2022).
83. EnergyPlus Manual 2021. Available online: https://energyplus.net/documentation (accessed on 21 September 2022).
84. Al-Samman, S.; Eftekhari, M.; Coakley, D.; Angelopoulos, C.; Dimitriou, V. *Sensor Location Methodology for Improved IEQ Monitoring in Working Environments*; ASHRAE: Atlanta, GA, USA, 2022.